Percolation of three-dimensional fracture networks with power-law size distribution

V. V. Mourzenko, J. -F. Thovert, P. M. Adler

Percolation of three-dimensional fracture networks with power-law size distribution

V. V. Mourzenko* and J.-F. Thovert†
LCD, SP2MI, BP 179, 86960 Futuroscope Cedex, France

P. M. Adler‡
IPGP, tour 24, 4 Place Jussieu, 75252 Paris Cedex 05, France

(Received 30 June 2004; revised manuscript received 14 June 2005; published 6 September 2005)

The influence of various parameters such as the domain size, the exponent of the power law, the smallest radius, and the fracture shape on the percolation threshold of fracture networks has been numerically studied. For large domains, the adequate percolation parameter is the dimensionless fracture density normalized by the product of the third moment of fracture radii distribution and of the shape factor; for networks of regular polygons, the dimensionless critical density depends only slightly on the parameters of radii distribution and on the shape of fractures; a model is proposed for the percolation threshold for fractures with elongated shapes. In small domains, percolation is analyzed in terms of the dimensionless fracture density normalized by the sum of two reduced moments of the radii distribution; this provides a general description of the network connectivity properties whatever the dominating percolation mechanism; the fracture shape is taken into account by using excluded volume in the definition of dimensionless fracture density.

DOI: 10.1103/PhysRevE.72.036103 PACS number(s): 02.50.−r, 61.43.Hv

I. INTRODUCTION

Fractures and fracture networks determine the permeability of many natural rocks, and their behavior generated interest in various fields; some aspects of this problem are discussed in, e.g., Sahimi [1], Adler and Thovert [2], and the National Research Council [3]. Recent advances in modeling of flow and transport phenomena in fractured rock are reviewed by Berkowitz [4].

Many studies focused on scaling behavior of fracture systems; several scaling laws have been proposed which relate various properties of these systems, namely geometrical, hydraulic, transport or mechanical on different scales. In many cases, no characteristic length in the statistical distributions of geometrical properties of rock fractures can be observed, and these distributions are shown to follow a power law. This can result in the dependency of connectivity of fracture systems on scale [5]. A thorough survey of power law scalings proposed for natural fracture systems together with their range of applications is presented by Bonnet *et al.* [6].

Moreover, two features render the situation still more complex. The first one is that the shape of the fractures is unknown and is likely to vary from element to element. The second one is that the larger fractures may be larger than the observation zone.

Percolation of random systems has been the topic of many studies in the past [7]. The percolation threshold is a property which depends on the details of the random system; in this sense, it is not universal in contrast with critical exponents which depend mostly on the space dimension. However, the percolation threshold is crucial for the transport properties. For instance, below the percolation threshold the permeability of a fracture network is equal to zero. For this reason, a lot of attention has been devoted in the past to percolation properties of fracture networks. Percolation in two-dimensional (2D) systems of line segments with lengths uniformly distributed in a finite interval was analyzed by Robinson [8,9]; it was shown numerically that the critical line density is proportional to the second moment of the line size distribution. Three-dimensional (3D) systems of discs were considered by Charlaix *et al.* [10], who proposed an invariant percolation parameter for polydisperse networks defined as the product of the fracture network density and of the third moment of fracture size distribution.

Huseby *et al.* [11] used the concept of excluded volume to obtain percolation thresholds independent of the fracture shape for monodisperse networks. Because of its importance, this study will be detailed in Sec. II A. de Dreuzy *et al.* [12] considered the connectivity of three-dimensional systems of ellipses of various aspect ratios. They found that a scale invariant percolation parameter is the union of the mutual excluded volumes of all ellipses in the system per unit volume which is proportional to the third moment of the length distribution. Fluctuations of this percolation parameter at the threshold with the power law exponent and the eccentricity have been shown numerically to remain limited within a range of less than one order of magnitude.

Rossen *et al.* [13] considered the dependence of the connectivity of power law fracture systems on the observation volume size.

Percolation in fractured networks with a broad distribution of sizes is a part of a more general multimodal continuum percolation problem. Lorenz *et al.* [14] analyzed the percolation properties of systems of discs in 2D or spheres in 3D with single or uniformly distributed radii. They demonstrated that the percolation threshold, in terms of the volume fraction of the randomly placed objects, is larger in the case of multimodal radii distribution than for the model with

*Electronic address: murzenko@lcd.ensma.fr
†Electronic address: thovert@lcd.ensma.fr
‡Electronic address: adler@ipgp.jussieu.fr

equally sized disks or spheres. The problem of the dependence of continuum percolation thresholds on polydispersity has also been addressed by Berkowitz [15], Dhar [16], Mecke and Seyfried [17], and Consiglio *et al.* [18].

This paper is an extension of the studies of Huseby *et al.* [11] to networks of polydisperse fractures distributed according to a power law. Moreover, the size of the system is not necessarily large when compared to the largest fractures. This paper complements our recent presentation [19] which addressed the permeability of such systems. The present contribution is organized as follows. In Sec. II, the geometrical model of polydisperse fractures is described, the numerical approach is briefly discussed. The percolation behavior of monodisperse networks is recalled; various dimensionless fracture network density definitions are given for polydisperse systems; two forms of percolation probability functions based on the error function and on the exponential dependence are presented. Numerical results for large domains whose size exceeds the maximum fracture diameter, are given in Sec. III. The influence of the parameters of the radii distribution and fracture shapes on the percolation threshold as well as the finite size effects are discussed. In Sec. IV, percolation properties of small parts of fracture networks are considered, when the domain size is smaller than the maximum fracture diameter; an adequate choice of the dimensionless fracture density in this case is discussed; various percolation mechanisms are analyzed depending on the system size and on the parameters of fracture radii distribution. The variations of the percolation threshold with the scale as well as the transition between small samples and large domains are considered in Sec. V. Some concluding remarks in Sec. VI complete this paper.

II. GENERAL

We consider three-dimensional networks made up of fractures with plane polygonal shapes. These polygons may be regular or not, but all their vertices are supposed to lie on their circumscribed circle, whose radius R provides a measure of their size. In agreement with many observations of fractured rocks [2], the statistical distribution of the fracture sizes is supposed to be described by a power law

$$n(R) = \alpha R^{-a}, \tag{1}$$

where $n(R)dR$ is the probability of fracture radii in the range $[R, R+dR]$; α is a normalization coefficient, and the exponent a ranges between 1 and 5. In practice, R may vary over a large interval which can span five orders of magnitude, from the size R_m of the microcracks to the size R_M of the largest fractures in the system. The normalization condition implies that α verifies

$$\alpha = \frac{a-1}{R_m^{1-a} - R_M^{1-a}} \quad (a \neq 1), \tag{2a}$$

$$\alpha = \frac{1}{\ln R_M - \ln R_m} \quad (a = 1). \tag{2b}$$

According to a recent synthesis on the real distribution of fracture trace lengths in a plane intersecting a three-dimensional fracture network, the corresponding exponent a_{2D} varies between 0.8 and 3.5 with a maximum occurrence around 2.0 [6]. Piggott [20] argued via an analytical development that the exponents a_{2D} and a are related by $a = a_{2D} + 1$; a similar observation in numerical simulations has been presented by Berkowitz and Adler [21]. Thus, it is reasonable to assume that a varies between 1.8 and 4.5 with a maximum likelihood around 3.0.

The percolation properties of such networks are investigated in a finite cubic domain Ω of size L^3. Hence, two main cases can be distinguished, when R_M is significantly smaller or larger than the domain size L; in addition, a transition regime takes place when R_M and L are of comparable orders of magnitude. In all cases, it is supposed that R_m is much smaller than L.

The first task to be performed, and may be conceptually the essential one, is the derivation of an adequate definition of the network density.

A. Monodisperse networks

Let us briefly recall at this stage the approach and the main results of a previous investigation of the percolation properties of fracture networks [11]. It was conducted by using the same procedures and numerical tools as in the present case, for networks made up of randomly oriented plane polygonal fractures with identical sizes. Various fracture shapes were considered, namely ν-sided regular polygons ($\nu = 3$ to 20) and rectangles with an aspect ratio equal to 2.

For monodisperse fracture sizes, the volumetric number density ρ is obviously a convenient characterization of the network density. In order to obtain intrinsic results, i.e., invariant within a change of scale, the cubed fracture radius R^3 can be used as the unit volume, so that ρ is the number of fractures per volume R^3. For any given fracture shape, a critical density ρ_c, corresponding to the onset of percolation, can be determined in these terms. However, the critical densities for different shapes greatly differ, e.g., $\rho_c \approx 1.9$ for 20-gones and $\rho_c \approx 5.4$ for triangles. This is mostly due to the arbitrary character of the parameter R which is used to quantify the fracture size, and of the unit volume R^3 upon which the definition of the network density is based.

It should also be noted that two definitions of the network density appear possible. One is volumetric, quantified by the average number of fractures in a reference volume; the other is topological, defined as the average number of connections per fracture with other fractures in the network, i.e., a mean coordination number. These two quantities are proportional one to another for a given fracture shape, but their ratio strongly depends on the shape if the reference volume is not properly defined.

However, the two definitions are nicely reconciled by the concept of excluded volume, which was introduced in the context of continuum percolation by Balberg *et al.* [22]; note that this concept has been used for a longer time in other fields (see Refs. [23,24]).

For a pair of objects F_1 and F_2, with given shapes and orientations, the excluded volume V_{ex} is the volume in which

the center of F_2 must be relative to the center of F_1 in order for F_1 and F_2 to intersect. For instance, F_1 and F_2 are spheres with radii R_1 and R_2, the excluded volume is a sphere with radius R_1+R_2. It can be shown (see Ref. [2]) that if the objects are two-dimensional, with areas A_i, perimeters P_i ($i=1,2$), random orientations and convex contours, their excluded volume is

$$V_{\mathrm{ex},12} = \tfrac{1}{4}(A_1P_2 + A_2P_1). \tag{3}$$

This is a particular case of the kinematic formula for convex bodies [25,26]. If all the polygons are identical, (3) reduces to

$$V_{\mathrm{ex}} = \tfrac{1}{2}AP. \tag{4}$$

An anisotropic orientation distribution can easily be accounted for in the evaluation of the excluded volume, as shown by Ref. [2].

We may use V_{ex} to define the dimensionless fracture density ρ',

$$\rho' = \rho\, V_{\mathrm{ex}}. \tag{5}$$

It can be interpreted as a volumetric density, since it is the number of fractures per volume V_{ex}; however, it also represents the mean number of intersections per fracture with other fractures in the network, and as such, it is a direct measure of the connectivity. Therefore, the definition (5) incorporates both the volumetric and topologic aspects mentioned above.

This definition proved very successful in unifying the critical densities of networks of fractures with different shapes. For regular polygons with 3 to 20 vertices, as well as for rectangles with aspect ratio two, Huseby *et al.* [11] obtained a nearly constant percolation threshold

$$\rho'_c = 2.26 \pm 0.04. \tag{6}$$

It was also shown that many other geometrical features, such as the volumetric density of blocks or the cyclomatic number only depend on the density ρ'. Furthermore, Koudina *et al.* [27] showed that the permeability of networks made up of fractures with various shapes, including the previous ones and polygons with 4 to 20 vertices randomly distributed on a circle, can also be expressed as a function of ρ' only.

Hence, it appears that the percolation threshold of monodisperse fracture networks, as well as many other properties, only depend on ρ', that is on the mean number of connections per fracture.

B. Polydisperse networks

Aside from the fracture shape, and from their orientation which is taken here randomly and isotropically distributed, the contents of the fracture networks can be characterized by the three parameters R_m, R_M and a associated with the size distribution [see Eqs. (1) and (2)] and some measure of the network density.

Obviously, the global volumetric number density of fractures ρ is inappropriate, since it makes no distinction between the smallest and the largest fractures in the system. In addition, it seems desirable to design a measure of the density that can be varied independently of the three other parameters R_m, R_M, and a, so that we may for instance investigate the influence of the lower cutoff R_m without changing any other parameter.

To this end, we introduce the volumetric number density of fracture per fracture size $F(R)$,

$$F(R) = \rho n(R), \tag{7}$$

where $F(R)dR$ is the number of fractures with radius in the range $[R, R+dR]$ per unit volume.

The volumetric moments M_p of the fracture radii are defined as

$$M_p = \int_{R_m}^{R_M} R^p F(R) dR. \tag{8}$$

They can be expressed as

$$M_p = \rho\alpha \frac{R_M^{p+1-a} - R_m^{p+1-a}}{p+1-a} \quad (a \neq p+1), \tag{9a}$$

$$M_p = \rho\alpha(\ln R_M - \ln R_m) \quad (a = p+1). \tag{9b}$$

Hence, the moments of the radii $\langle R^p\rangle = M_p/M_0$ are given by

$$\langle R^p\rangle = \frac{1-a}{p+1-a} \frac{R_M^{p+1-a} - R_m^{p+1-a}}{R_M^{1-a} - R_m^{1-a}} \quad (a \neq 1, p+1). \tag{10}$$

The value of $\langle R^p\rangle$ for $a=1$ or $p+1$ can be obtained by combining (9a) and (9b).

For monodisperse fracture networks, the dimensionless density ρ' (5) was shown to characterize well the connectivity of systems of fractures with various polygon shapes, and to provide a unique value for the percolation threshold. For the networks under consideration here which are made up of fractures with identical shapes but different sizes, it is convenient to express the excluded volume V_{ex} in Eq. (3) as the product

$$V_{\mathrm{ex}} = v_{\mathrm{ex}} \frac{R_1R_2^2 + R_1^2R_2}{2}, \tag{11}$$

where v_{ex} is a dimensionless shape factor, equal for instance to π^2 for disks, $9\sqrt{3}/2$ for hexagons, and $4\sqrt{2}$ for squares. It is the introduction of this shape factor in the density ρ' that allowed to unify the description of the percolation and transport properties of monodisperse networks of fractures with various shapes. Therefore, this feature is kept in the definitions of the three dimensionless densities that are used in the following:

$$\rho'_0 = \rho v_{\mathrm{ex}} R_M^3, \tag{12a}$$

$$\rho'_{21} = \rho v_{\mathrm{ex}} \langle R^2\rangle \langle R\rangle, \tag{12b}$$

$$\rho'_3 = \rho v_{\mathrm{ex}} \langle R^3\rangle, \tag{12c}$$

where the brackets $\langle\ \rangle$ denote the statistical moments of R weighted by $n(R)$. The subscripts are reminders of the statistical moments involved in each definition. The first one, ρ'_0,

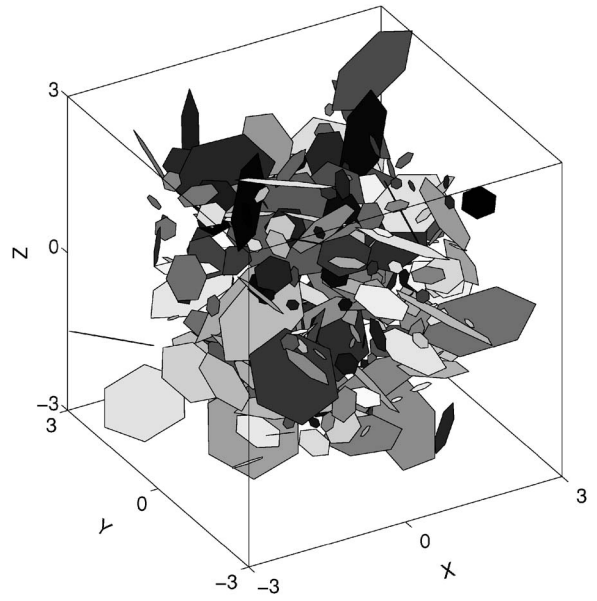

FIG. 1. Example of polydisperse network of hexagonal fractures, with $L'=4$, $a=1.5$, $R'_m=0.1$, which contains $N_{\mathrm{fr}}=300$ fractures ($\rho'_{21}=26.5$, $\rho'_0=1.25$, $\rho'_3=2.44$). The unit for the coordinates is R_M.

is the simplest definition, based on the single length scale R_M, but it cannot be expected to capture the scaling character of the network. The second one is the generalization of ρ' for monodisperse networks, since it can be shown that it still is equal to the mean number of intersections per fracture [2]. It is therefore a candidate to be considered, but it turns out that this measure of the local connectivity does not control the global network percolation and that the last one ρ'_3 is much more successful in this respect.

The generation and analysis of the percolation properties of fracture networks are similar to those presented by Huseby *et al.* [11]. The fractures are embedded in the cubic domain Ω of size L; $N_{\mathrm{fr}}=\rho L^3$ is the number of fractures in Ω. Fracture centers are uniformly distributed in space, and their normal vectors are uniformly distributed on the unit sphere.

Two types of fracture systems were used in the calculations depending on the boundary conditions. First, nonperiodic networks were tested and the percolation cluster must touch opposite faces of the domain along, say, the x direction. In this case, fracture centers were generated within Ω as well as outside it provided that the incoming fractures intersect at least one of the six faces of the domain. An example is shown in Fig. 1. Second, when $R_M<L/2$, spatially periodic networks were generated; all fracture centers lie in the interior of Ω, which is the unit cell of a spatially periodic network; in addition the percolation cluster must contain two homologous fractures, i.e., two fractures with the same coordinates, modulo the period L along the x direction.

Three length scales define two dimensionless ratios,

$$R'_m=\frac{R_m}{R_M}, \quad L'=\frac{L}{R_M} \tag{13}$$

which together with the exponent a determine the connectivity and percolation properties of the fracture networks. In order to eliminate the influence of the lower cutoff R_m, the first ratio in (13) is kept as small as possible, while the second one is systematically varied.

For given values of ρ', L', R'_m, and a, where ρ' denotes any one of the dimensionless densities defined in (12) or simply ρ, the probability $\Pi(L',\rho')$ of having a percolating cluster which spans the domain along the x direction, is derived from N_r realizations of the system; then, the value $\rho'_c(L')$ for which $\Pi=0.5$ is estimated. In all the tests, the value $N_r=500$ is used. Π and ρ'_c depend on five or four parameters as summarized by the formulas

$$\Pi(R'_m,L',a,\mathcal{S},\rho'), \quad \rho'_c(R'_m,L',a,\mathcal{S}), \tag{14}$$

where $\mathcal{S}$ denotes the fracture shape. For brevity, they will be often written as

$$\Pi(L'), \quad \rho'_c(L'). \tag{15}$$

A particular choice of the density ρ' among (12), ρ or any other measure is not important for the estimation of the percolation threshold, because for fixed values of R'_m and a, they differ one from another by constant factors only.

In the limit of large L', the fracture networks are expected to follow the standard percolation theory with the percolation threshold $\rho'_c(\infty)$ [7],

$$\rho'_c(L')-\rho'_c(\infty)\propto L'^{-1/\nu}, \tag{16}$$

where ν is the critical exponent. In our estimations of $\rho'_c(L')$, the data for $\Pi(L',\rho')$ were fitted by a two-parameter error function of the form [cf. Fig. 2(a)]

$$\Pi(L',\rho')=\frac{1}{\sqrt{2\pi}}\int_{-\infty}^{\rho'}\frac{1}{\Delta_L}\exp\left(-\frac{[\xi-\rho'_c(L')]^2}{2(\Delta_L)^2}\right)d\xi, \tag{17}$$

where Δ_L is the width of the transition region of $\Pi(L',\rho')$ which follows a scaling relation in the limit of large L':

$$\Delta_L\propto L'^{-1/\nu}. \tag{18}$$

When L' increases, Δ_L tends to zero. Therefore, in infinite systems, Π switches abruptly from zero to one when ρ exceeds some critical density, and percolation is a critical phenomenon.

For small L', when a single fracture is able to span the whole domain, the percolation probability Π can never totally vanish, no matter how small the density ρ. Therefore, the notions of critical density and of percolation phase transition are not applicable. Still, it might be of practical interest to investigate the probability of a finite system to contain a spanning cluster. Hence, we also consider the density ρ'_c for which Π is equal to $1/2$, and by lack of a better word, we still call it the percolation threshold for a system with given characteristics and size. However, it is understood that it is only a transition between Π smaller or larger than $1/2$.

In general, the percolation probability $\Pi(L',\rho')$ in small domains does not follow the error function (17). Numerical simulations showed that, at least for $a<3$, it can be fitted instead by the one-parameter exponential function [cf. Fig. 2(b)]

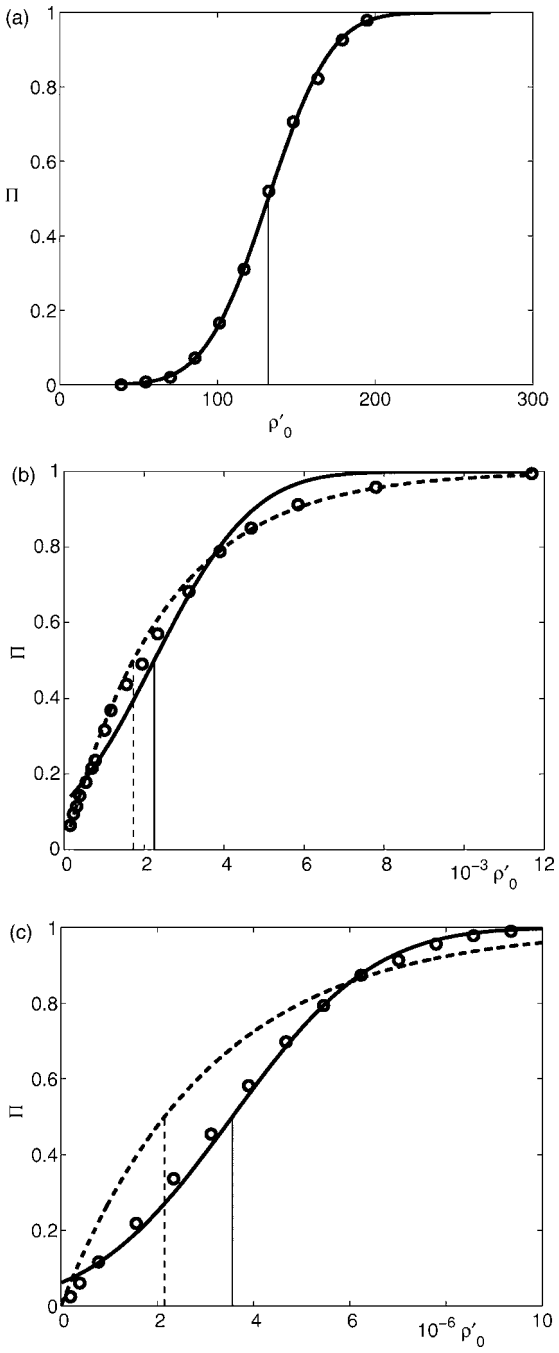

FIG. 2. Percolation probability Π versus fracture number density for networks of regular hexagons. Data are for $a=1.5$, $L'=4$, and $R'_m=0.01$ (a), $a=1.5$, $L'=0.1$, $R'_m=0.003\,125$ (b), and $a=3.5$, $L'=0.1$, $R'_m=0.003\,125$ (c). (○) correspond to the numerical data, (—) to a fit by an error function, Eq. (17), (---) to a fit by an exponential function, Eq. (19). Vertical lines show estimated percolation thresholds $\rho_c(L)$ corresponding to these two fits.

$$\Pi(L',\rho') = 1 - \exp\left(-\frac{\rho' \ln 2}{\rho'_c(L')}\right). \tag{19}$$

This was used, whenever possible, to determine ρ'_c from the numerical data.

When the percolation probability follows neither the Gaussian law (17) nor the Poisson law (19), which occurs when L' is of the order of unity, or when $L'<1$ and $3\leqslant a \leqslant 4$ [see (34)], the value of ρ'_c can be evaluated directly from a linear interpolation of numerically calculated $\Pi(L',\rho')$ near $\Pi=0.5$. This approach was found to be stable enough and it has been applied when both (17) and (19) failed.

III. LARGE DOMAINS

In order to analyze the percolation properties of fracture networks in the case of large domains ($L'\gg 1$), the influence of R'_m and a is first analyzed for hexagonal fractures with fixed L'. Then, the finite size effects are discussed for networks of fractures of various shapes when $R'_m=1$ or 0.1.

A. Influence of R'_m for hexagons

Let us start with R'_m whose influence on the percolation threshold is displayed in Fig. 3. Three different definitions of the critical fracture network density are considered, namely the thresholds $\rho'_{3c}(L')$, $\rho'_{21c}(L')$, and $\rho'_{0c}(L')$ associated with the three dimensionless densities of Eq. (12). They give rise to very different trends. The most natural extension of ρ'_c, namely ρ'_{21c}, turns out to be an increasing function of R'_m, while ρ'_{0c} is decreasing. However, ρ'_{3c} does not vary much as it is seen in Fig. 3(c); when R'_m decreases from 1 down to 0.5, ρ'_{3c} decreases from 3 down to 2.9; when R'_m decreases further to 10^{-2}, ρ'_{3c} increases slightly to reach a constant value which is almost independent of a.

Let us concentrate on ρ'_{3c} since it has the crucial advantage to be almost independent on a and R'_m, and consider in more details the results in Fig. 3(c) (see also Table I). For the time being, we shall only consider the data for $L'=4$. It is interesting to note that the spatially periodic or aperiodic character of the networks has only a very small influence on ρ'_{3c}. In this figure, the influence of a appears to be very weak with the exception maybe of $a=2.9$ when $R'_m\to 0$. It should be said that in this limit ρ'_{3c} has not yet reached an asymptotical value when R'_m has decreased to 0.03; this is probably because the influence of the smallest fractures is slower to vanish, since their proportion is very large for $a=2.9$.

B. Influence of a for hexagons

The variations of $\rho'_{3c}(L')$ with a are shown in Fig. 3(d). The percolation threshold is fairly constant in the range $1.5<a<4$; it starts decreasing slightly for $a>4$. This can be attributed, perhaps, to the finite size effect, which decreases for large a due to the decrease of the mean fracture size and the resulting increase of the effective domain size.

Periodic networks consistently yield lower thresholds than nonperiodic networks, but only by a small amount of the order of 0.03.

As a whole, all the data in Figs. 3(c) and 3(d) for $L'=4$ fall in a fairly narrow range,

$$\rho'_{3c}(L'=4) = 2.95 \pm 0.12. \tag{20}$$

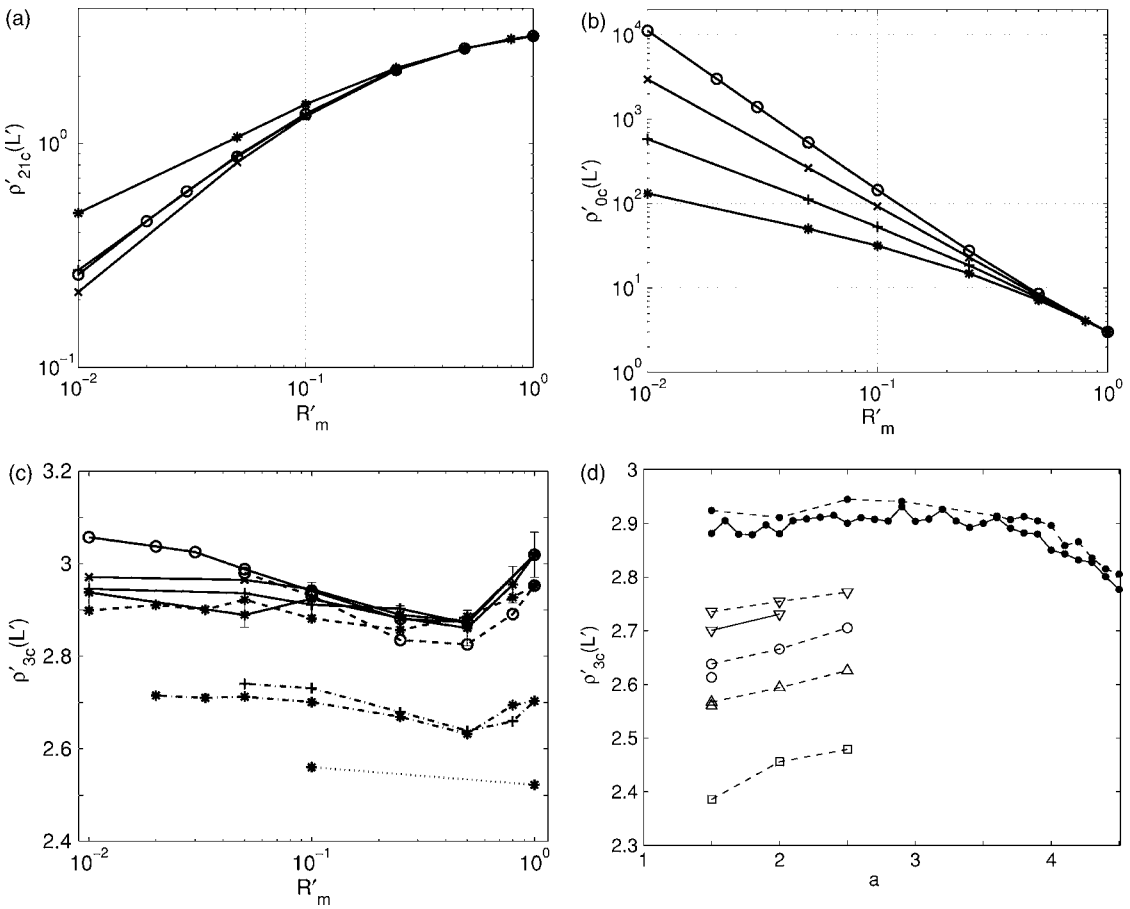

FIG. 3. Percolation thresholds expressed in terms of the densities $\rho'_{21c}(L')$ (a), $\rho'_{0c}(L')$ (b), and $\rho'_{3c}(L')$ (c) for regular hexagons versus R'_m. The symbols correspond to $a=1.5$ (*), $a=2$ (+), $a=2.5$ (×), and $a=2.9$ (○). The line types correspond to nonperiodic networks with $L'=4$ (—) and periodic networks with $L'=4$ (---), $L'=6$ (.-.-.-), and $L'=10$ (···). The threshold $\rho'_{3c}(L')$ is plotted versus a in (d), for nonperiodic (---) and periodic (—) networks with $R'_m=0.1$, and for $L'=4$ (●), $L'=6$ (▽), $L'=8$ (○), $L'=10$ (periodic) or 12 (nonperiodic) (△), and extrapolated for infinite systems (□) of hexagons.

These data were obtained for various values of the lower cutoff ($10^{-2} \leqslant R'_m \leqslant 1$), and of the exponent ($1.5 \leqslant a \leqslant 3$). Periodic and nonperiodic boundary conditions were also used.

C. Discussion for hexagons

The fact that the percolation threshold presented in terms of ρ'_3 does not vary with R'_m for small R'_m indicates that, probably, the largest fractures in the system control the connectivity of the network. This can be rationalized as follows.

When R_M and ρ'_0 are kept constant and R_m decreases, the same number of fractures is spread over a wider range of size, and large fractures are replaced by smaller ones. For instance, it follows from Eqs. (1), (2), and (7) that the density of the largest fractures decreases as

$$F(R_M) \sim R_m^{a-1}. \tag{21}$$

This is obviously unfavorable for percolation and therefore ρ'_{0c} must increase when R_m decreases, as observed in Fig. 3(b).

If instead ρ'_{21}, i.e., the mean number of intersections per fracture, is kept constant and R_m decreases, it implies that the number of large fractures (with many intersections) increases, in order to compensate for the larger number of small fractures with less than the average intersections. Specifically,

$$F(R_M) \propto R_m^{1-a}, \quad 1 < a < 2, \tag{22a}$$

$$F(R_M) \propto R_m^{-1}, \quad 2 < a < 3, \tag{22b}$$

$$F(R_M) \propto R_m^{a-4}, \quad 3 < a < 4. \tag{22c}$$

This favors percolation and therefore ρ'_{21c} decreases when R_m decreases, as seen in Fig. 3(a).

Finally, both $\langle R^3 \rangle$ and the density of large fractures scale as R_m^{a-1} for $1<a<4$. This means that the density of large fractures is nearly unaffected when R_m decreases and ρ'_3 is kept constant. In other words, the density ρ'_3 is almost insensitive to the value of the lower cutoff R_m, provided that it is much smaller than R_M. Since the threshold $\rho'_{3c}(L')$ is also nearly independent of R_m in Fig. 3(c), it suggests that for $a<4$ percolation relies on the upper part of the fracture size spectrum.

TABLE I. Percolation thresholds $\rho'_{3c}(L')$ of fracture networks, for various cell sizes L'. Numbers in parentheses are 95% confidence intervals.

$\rho'_{3c}(L')$ for	$L'=4$	$L'=6$	$L'=8$	$L'=10$	$L'=12$	$L'=20$	$L'\to\infty$
Periodic networks of hexagons, $R_m=0.1$							
$a=1.5$	2.88 (0.04)	2.70 (0.03)	2.61 (0.03)	2.56 (0.03)			2.39 (0.03)
$a=2.0$	2.88 (0.03)	2.73 (0.02)					2.48 (0.07)
Monodisperse	2.95 (0.05)	2.70 (0.03)		2.52 (0.02)		2.41 (0.01)	2.31 (0.013)
Nonperiodic networks of hexagons, $R_m=0.1$							
$a=1.5$	2.92 (0.04)	2.74 (0.03)	2.64 (0.02)		2.57 (0.02)		2.39 (0.03)
$a=2.0$	2.91 (0.05)	2.75 (0.03)	2.67 (0.02)		2.59 (0.02)		2.46 (0.03)
$a=2.5$	2.95 (0.04)	2.77 (0.03)	2.71 (0.02)		2.63 (0.02)		2.48 (0.03)
$a=2.9$	2.94 (0.03)						
$a=3.6$	2.91 (0.03)						
$a=4.0$	2.90 (0.03)						
$a=4.5$	2.81 (0.02)						
Monodisperse	3.02 (0.06)	2.83 (0.04)	2.63 (0.03)		2.53 (0.02)	2.43 (0.01)	2.31 (0.015)
Nonperiodic networks of triangles, $R_m=0.1$							
$a=1.5$	2.69 (0.03)	2.58 (0.03)	2.51 (0.02)		2.46 (0.01)		2.35 (0.013)
Monodisperse	2.80 (0.04)	2.60 (0.03)	2.51 (0.01)		2.40 (0.02)	2.34 (0.01)	2.24 (0.01)
Nonperiodic networks of squares, $R_m=0.1$							
$a=1.5$	2.82 (0.03)	2.69 (0.02)	2.61 (0.02)		2.55 (0.01)		2.42 (0.014)
Monodisperse	2.96 (0.05)	2.72 (0.04)		2.53 (0.03)		2.42 (0.01)	2.31 (0.014)
Nonperiodic networks of hexagons and rectangles with aspect ratio 4, 50%–50%, $R_m=0.1$							
$a=1.5$		2.47 (0.02)					
Monodisperse		2.47 (0.03)					
Nonperiodic networks of hexagons and triangles, 50%–50%, $R_m=0.1$							
$a=1.5$		2.59 (0.02)					
Monodisperse		2.62 (0.03)					
Nonperiodic monodisperse networks of rectangles with aspect ratio h/w.							
$h/w=1$	2.96 (0.05)	2.72 (0.04)		2.53 (0.03)		2.42 (0.01)	2.31 (0.014)
$h/w=2$	2.85 (0.04)	2.61 (0.03)		2.41 (0.02)		2.32 (0.01)	2.20 (0.01)
$h/w=4$	2.45 (0.03)	2.24 (0.03)		2.13 (0.01)		2.06 (0.01)	1.99 (0.01)
$h/w=8$	2.01 (0.02)	1.89 (0.02)		1.83 (0.01)		1.79 (0.01)	1.74 (0.01)
$h/w=16$	1.65 (0.01)	1.60 (0.01)		1.57 (0.01)		1.55 (0.01)	1.53 (0.01)

D. Influence of L' ($L'\gg 1$) for hexagons

Consider now the influence of the sample size L' on the connectivity of the fracture networks. Figure 3(c) also shows systematic results for periodic fracture systems with $L'=6$. A comparison with the data for $L'=4$ shows that the finite-size effects persist for this value of the sample size. Larger domain sizes have been considered for $a=1.5$, 2, and 2.5 as well as for monodispersed networks, in order to conduct a finite-size analysis [see Fig. 3(d) and Table I].

As already stated, the spatially periodic character of the networks plays only a minor role [see Fig. 3(d)]. Furthermore, the influence of this boundary condition decreases with the sample size, as could be expected.

A small dependence of $\rho'_{3c}(L')$ on the exponent a is observed when $L'\geqslant 6$, but of a small amplitude. For instance, it increases by 2%, from 2.57 for $a=1.5$ to 2.63 for $a=2.5$, when $L'=12$.

Figure 4(a) shows the percolation threshold as a function of the width of the transition zone Δ_L when the system size L' increases. According to the scaling relations of standard percolation theory (16) and (18), $\rho'_{3c}(L')$ linearly varies with Δ_L for large L',

$$\rho'_{3c}(L') - \rho'_{3c}(\infty) \propto \Delta_L. \tag{23}$$

Hence, one can evaluate the asymptotic limit $\rho'_{3c}(\infty)$ from the corresponding linear fit as an extrapolation of $\rho'_{3c}(L')$ for $\Delta_L \to 0$, without having to determine the critical exponent ν. Note that Δ_L quantifies the sharpness of the transition for each L', and therefore, it is by itself a measure of the uncertainty of the determination of $\rho'_{3c}(L')$.

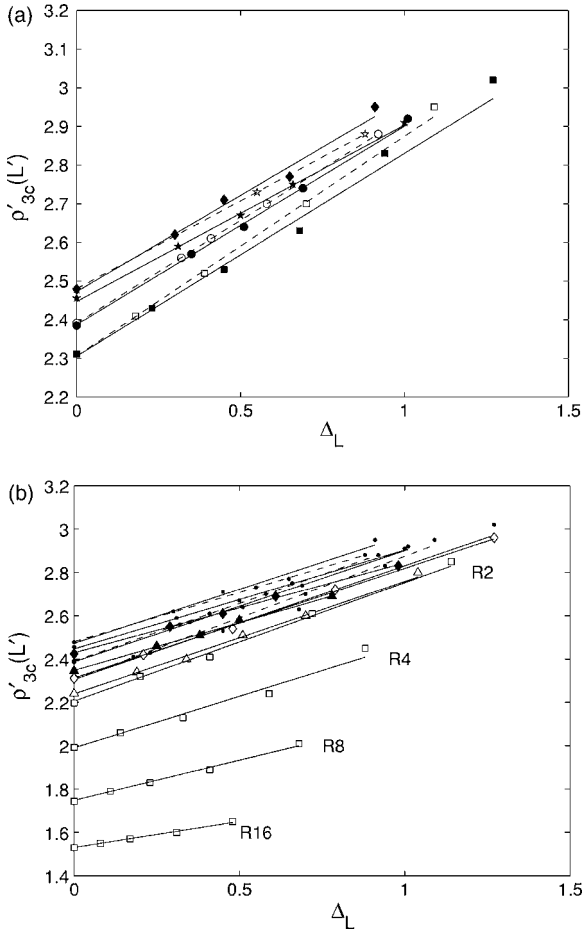

FIG. 4. The percolation threshold $\rho'_{3c}(L')$ as a function of the width Δ_L of the transition zone. Data in (a) are for periodic (open symbols) or nonperiodic (black symbols) networks of hexagons, monodisperse (□) or polydisperse with $R'_m=0.1$ and $a=1.5$ (○), 2 (★) or 2.5 (◇). Additional data are given in (b), for nonperiodic monodisperse (open symbols) or polydisperse with $a=1.5$ and $R'_m=0.1$ (black symbols) networks of triangles (△), squares (◇) and rectangles (□) with various aspect ratios 2, 4, 8, and 16. The dots are the data for hexagons also shown in (a). The lines in (a),(b) are the least square fits (23) and the symbols on the vertical axis are the extrapolated $\rho'_{3c}(\infty)$.

The extrapolated values for monodisperse networks and for polydisperse ones with $a=1.5$, 2, or 2.5 with $R'_m=0.1$ are given in Table I; for $L'=\infty$, ρ'_{3c} for polydisperse systems is slightly larger than for monodisperse ones, while the opposite is true for finite L'. This results from different prefactors of Δ_L in Eq. (23). However, the variations of the extrapolated $\rho'_{3c}(\infty)$ are of a small amplitude, as already observed in Fig. 3(d) for $1.5 \leqslant a \leqslant 4$ in finite domains.

The data in Fig. 4(a) are for a particular value $R'_m=0.1$ (except in the case of monodisperse networks). However, ρ'_{3c} was found nearly independent of R'_m in finite domains with $L'=4$ and 6, and we may safely assume that this can be extended to larger and infinite domains, since the finite size effects are induced primarily by the largest fractures. Summarizing these results, the percolation threshold $\rho'_{3c}(\infty)$ for monodisperse or polydisperse networks of hexagons can be

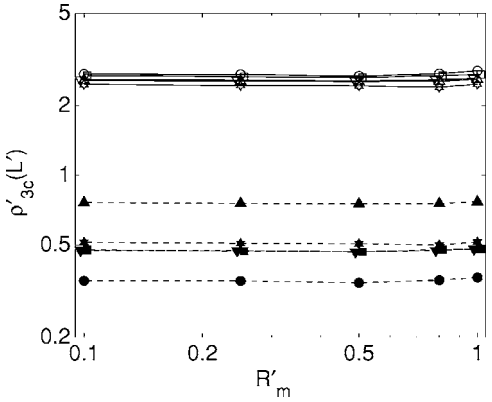

FIG. 5. The percolation thresholds ρ'_{3c} (open symbols, solid lines) and $\rho_c\langle R^3\rangle$ (black symbols, broken lines) for nonperiodic networks with $L'=6$ and $a=1.5$ for regular hexagons (○), squares (□), triangles (△), mixture of hexagons and triangles, 50%–50% (▽), and mixture of hexagons and rectangles with aspect ratio 4, 50%–50% (▽△).

expressed in a first approximation for any $R_m \leqslant 1$ and $1 \leqslant a \leqslant 4$ as

$$\rho'_{3c}(R'_m,a,\infty) = \rho'_{3c}(\infty) \approx 2.4 \pm 0.1. \tag{24}$$

E. Influence of the shape

Two kinds of shapes will be studied. The first one consists of regular polygons such as triangles, squares, and hexagons. The second one consists of rectangles with large aspect ratios.

Figure 5 displays ρ'_{3c} for networks with various fracture shapes. Two types of networks have been tested, namely networks with fractures of the same shape (hexagons, squares, or triangles) and mixtures containing hexagons and triangles (50%–50%) or hexagons and rectangles with aspect ratio 4 (50%–50%).

Note first that these data correspond to a range of cutoff radius $0.1 \leqslant R'_m \leqslant 1$. The small sensitivity of ρ'_{3c} to R'_m observed for hexagons in Fig. 3(c) is confirmed here for a variety of other fracture shapes.

The numerical data for all fracture shapes lie close one to another, although small but systematic deviations can be observed; the data for squares are below those for hexagons, and the data for triangles are below those for squares. The percolation threshold for mixtures of hexagons and other polygons is also smaller than for systems composed of hexagons only.

Nevertheless, for $L' \gg 1$, the dimensionless fracture density based on the shape factor v_{ex} successfully accounts for most of the influence of the fracture shape, especially for regular polygons. For instance, ρ'_{3c} for networks of hexagons, squares or triangles is within 2.66 ± 0.08 when $L'=6$, $a=1.5$, and $R_m=0.1$. In contrast, the data in Fig. 5 for $\rho_c\langle R^3\rangle$, which does not incorporate the shape factor, are very scattered.

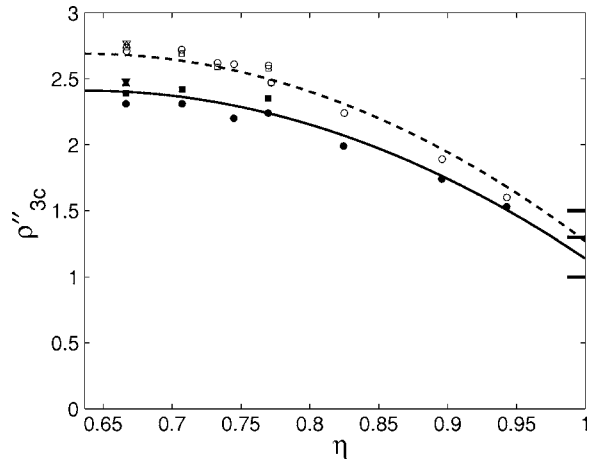

FIG. 6. The percolation thresholds ρ'_{3c} as functions of the shape factor η. Open symbols correspond to all the data for $L'=6$ in Figs. 4 and 5, for monodisperse (○) or polydisperse networks with $a=1.5$ (□), $a=2$ (△), and $a=2.5$ (▽). This includes hexagons, squares, triangles, mixtures of hexagons with rectangles or triangles, and rectangles with h/w up to 16. Black symbols correspond to the extrapolated values $\rho'_{3c}(\infty)$ in Fig. 4, with the same convention. The broken and solid lines are the models (25) and (26), respectively. The marks on the right vertical axis are the predictions of Refs. [28–30] for various kinds of elongated objects with infinite aspect ratios.

When polygons become elongated, the dependence of the percolation threshold on the aspect ratio becomes more important. This is clearly seen in Fig. 4(b) where data for monodisperse and polydisperse networks with $a=1.5$ in domains with increasing sizes L', with various fracture shapes, have been added to the results for hexagons of Fig. 4(a). The result for squares lies within the range of Eq. (24), but triangles yield a slightly lower value of $\rho'_{3c}(\infty)$. For rectangles, the threshold decreases significantly when the ratio of the length h to the width w increases.

This can be taken into account by using the shape factor $\eta=4R/P$ of the fractures. This ratio is minimum for disks, with $\eta=2/\pi\approx 0.637$, and it increases when the shape deviates from circularity. For rectangles it is equal to $\sqrt{h^2+w^2}/(h+w)$, and it ranges from $1/\sqrt{2}$ for squares to one for very long and narrow rectangles. It turns out that a quadratic correction in terms of the deviation of η from $2/\pi$ is very successful for the representation of the data for very different and irregular fracture shapes.

All the thresholds obtained in domains with $L'=6$ and monodisperse or polydisperse size distributions with $a=1.5$, 2, or 2.5 and $R_m=0.1$ are plotted in Fig. 6 as functions of η. This includes networks of hexagons, squares, triangles, mixtures of hexagons with rectangles or triangles, and rectangles with h/w up to 16. The data are well fitted by the expression

$$\rho'_{3c}(L')=2.69\left[1-4\left(\eta-\frac{2}{\pi}\right)^2\right] \quad (L'=6). \tag{25}$$

The deviations from this fit never exceed ±0.1. When fractures with different shapes coexist in the network, the mean value of the whole corrective term in square brackets in Eq. (25) is used, or equivalently, Eq. (25) applies with η replaced by $\bar{\eta}=2/\pi+\langle(\eta-2/\pi)^2\rangle^{1/2}$.

Finite size analyses have also been conducted for monodisperse and polydisperse networks of square and triangular fractures, and for monodisperse networks of rectangles with aspect ratios $h/w=2$, 4, 8, and 16. The results are given in Fig. 4(b) and Table I. For squares, the extrapolated value $\rho'_{3c}(\infty)$ is very close to that for hexagons, and within the range of Eq. (24). The result for triangles is only slightly smaller and below the lower limit of Eq. (24). Rectangular shapes yield much smaller values. However, the same kind of correction as in Eq. (25) can be made. A very good fit of all the data is provided by the following model, which extends Eq. (24) for all the shapes considered in this work

$$\rho'_{3c}(\infty)=2.41\left[1-4\left(\eta-\frac{2}{\pi}\right)^2\right]. \tag{26}$$

This model is plotted in Fig. 6 in comparison with numerical data. Again, the deviations never exceed ±0.1.

It can be noted that Eq. (26) predicts a threshold value 1.14 when h/w tends to infinity (i.e., when $\eta\to 1$), which is in the range of the predictions 1.5 of Ref. [28] for prolate ellipsoids, 1 of Ref. [29] for capped cylinders, and 1.3 of Ref. [30] for elongated prisms, in the limit of infinite slenderness.

IV. SMALL DOMAINS

The situations addressed in this section are out of the usual scope of percolation theory. For instance, as it was already mentioned in Sec. II B, they do not give rise to a critical phase transition. Recall also that the expression "percolation threshold" is used here in a loose sense, to refer to the density when percolation probability reaches 1/2. However, finite and even small domains are often encountered in practical applications, and it was thought worth giving them some consideration. For instance, one might be interested in the probability of existence of a percolating fracture network on a local scale (e.g., between a man-made structure and an aquifer), when large scale fractures are known to exist. Of course, some of the necessary data, such as ρ, R_M, and a cannot be obtained from observations on the local scale, but they might be available from other sources, such as a regional geological survey.

A. Single-fracture percolation

The main difference regarding the occurrence of percolation between the situations with $L'>2$ and $L'<2$ is the possibility in the latter case for a single fracture, possibly with its center outside the domain, to connect two opposite faces of Ω. This event results from a Poisson process, and therefore, the percolation probability function $\Pi(L',\rho')$ for small domains is not properly fitted any more by the error function (17) [see Fig. 2(b)].

Let us first note that the probability that a fracture with size in $[R,R+dR]$, area A and perimeter P intersects (not necessarily spans) Ω is

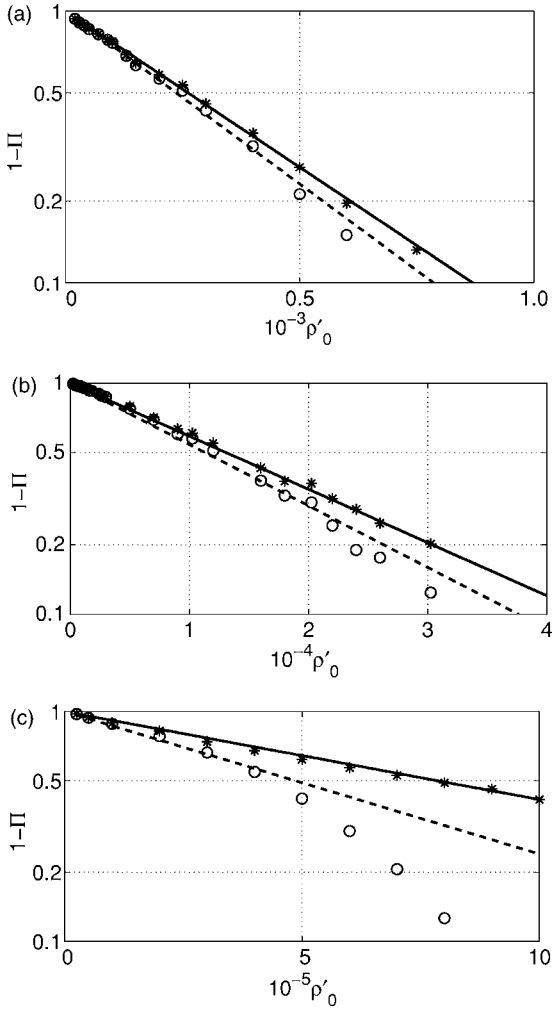

FIG. 7. The nonpercolation probability as a function of the fracture network density ρ'_0 for $L'=0.1$, $R'_m=0.003\,125$ and $a=1.5$ (a), 2.5 (b), and 3.5 (c). Data are for ○ ($1-\Pi$, nonpercolation probability of the whole network), ∗ ($1-\Pi_1$, probability of no single spanning fracture). The lines correspond to the exponential fit of the data for Π_1 (—) and to the prediction (30) (---).

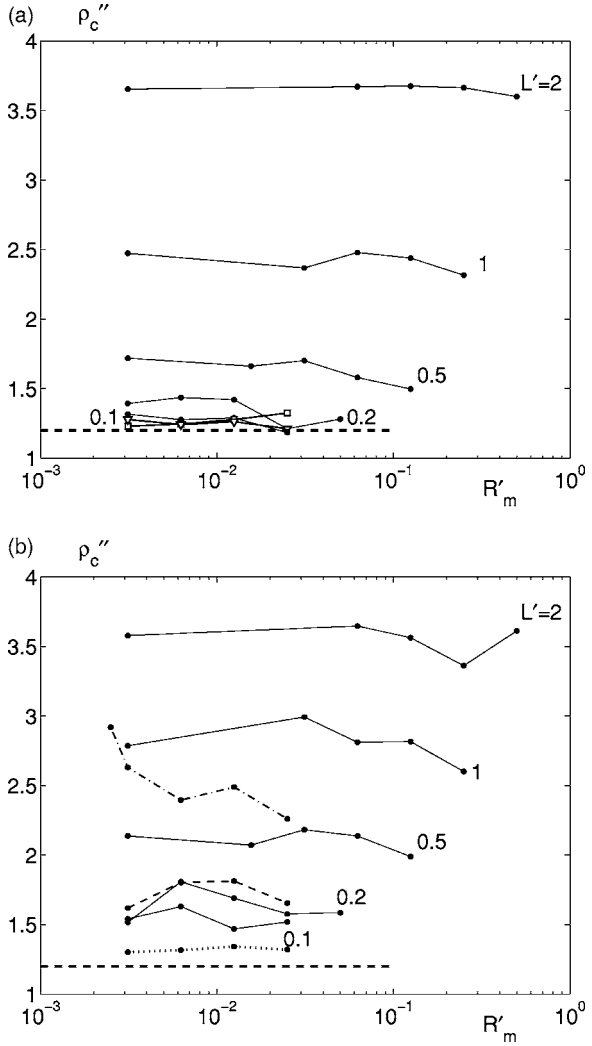

FIG. 8. The percolation thresholds ρ_c'' as functions of R'_m. Dots and solid lines (-•-) correspond to hexagons with $a=1.5$ (a) and 2.5 (b), in domains with sizes $L'=0.1$ to 2 indicated in the figure. Additional data are provided in (a) for squares (□) and triangles (▽) with $L'=0.1$ and $a=1.5$, and in (b) for hexagons with $a=2$ (···), 2.9 (---), and 3.5 (-.-.-). The horizontal dashed lines correspond to the prediction (32).

$$dp_I(R) = F(R)\left(\tfrac{3}{2}AL + \tfrac{3}{4}PL^2 + L^3\right)dR. \tag{27}$$

This is again a consequence of the kinematic formula [26]. Regardless of the fracture shape, this expression is dominated when R/L is large by its first term,

$$dp_I(R) \approx \tfrac{3}{2}LAF(R)dR \quad (L \ll R). \tag{28}$$

However, the probability that a fracture not only intersects the domain but also spans two of its opposite faces is smaller. In the limit of large fractures, it is given by (see the Appendix)

$$dp(R) \approx \frac{1}{\sqrt{3}}LAF(R)dR \quad (L \ll R). \tag{29}$$

This result was obtained by using the same approximation as when going from Eq. (27) to Eq. (28), i.e., by neglecting the intersections of Ω with the fracture near its border line compared to the intersections in the interior of its surface, and therefore, it also applies regardless of the fracture shape, in the limit $L \ll R$.

Since the fractures are supposed to be randomly located according to a Poisson process, the intersections of Ω by different fractures are independent events, and the overall probability $1-\Pi_1$ that percolation does not occur due to a single spanning fracture can be tentatively estimated as

$$1 - \Pi_1 = \exp\left(-\int p(R)dR\right) \approx \exp\left(-\frac{1}{\sqrt{3}}LA_p\rho\langle R^2\rangle^+\right), \tag{30}$$

where A_p is the shape factor A/R^2 of the polygon and

$$\langle R^2\rangle^+ = \int_{L/2}^{R_M} R^2 n(R)dR = \alpha\frac{R_M^{3-a} - (L/2)^{3-a}}{3-a}. \tag{31}$$

The percolation probability Π_1 for the existence of at least one spanning fracture is the complementary function to (30), and it can be written exactly in the form of (19) with

$$\rho' = \rho A_p L \langle R^2 \rangle^+ \quad \rho'_c = \sqrt{3} \ln 2 \approx 1.20. \tag{32}$$

Equations (30) or (19) and (32) quantify the probability of percolation in small domains when most fractures are larger than L, in terms of a single shape-independent quantity $\rho A_p \langle R^2 \rangle^+$. This is simply the volumetric area of fractures with $R \geqslant L/2$, which can be obtained from one-dimensional (line surveys) or two-dimensional (trace maps) field data [31,32].

Note however that Eq. (28) has been applied here somewhat beyond its range of validity, since the integration range in Eq. (31) violates the criterion $L \ll R$. The magnitude of the relative error is of the order of L'^{3-a}. Therefore, the prediction (32) is not expected to apply accurately when a is of the order of 3 or larger. Figure 7 shows (30) for three values of a; as expected, the prediction fits well the data for $a=1.5$; it is still good for networks with $a=2.5$. When $a=3.5$ the difference between (30) and the numerical data is substantial, although the dependence of Π_1 on the fracture density remains of the exponential form of (30) or (19).

B. Unified formulation

It is helpful to introduce a single percolation parameter, applicable over the whole range of the domain sizes. The following sum is a natural candidate:

$$\rho'' = \rho \left(v_{\mathrm{ex}} \int_{R_m}^{L/2} R^3 n(R) dR + A_p L \int_{L/2}^{R_M} R^2 n(R) dR \right)$$
$$= \rho v_{\mathrm{ex}} \left(\langle R^3 \rangle^- + \frac{\eta L}{2} \langle R^2 \rangle^+ \right). \tag{33}$$

It reduces to ρ'_3 when no fracture larger than L exists ($L' > 2$), and to ρ' in (32) when the contribution of the small fractures can be neglected.

A set of results is presented in these terms in Fig. 8, for domains with $L'=0.1$ to 2. The value of ρ''_c is plotted as a function of the lower cutoff radius R'_m. In all cases with $a < 3$, ρ''_c is found independent of R'_m. Additional data for square and triangular fractures in Fig. 8(a) confirm that ρ''_c does not depend either on the fracture shape when $L' \ll 1$. As the domain size decreases, ρ''_c converges as expected to the limit $\sqrt{3} \ln 2$ [see Eq. (32)], although this convergence gets slower when the exponent a increases (see also Fig. 10). For $a > 3$, ρ''_c depends on R'_m and it is not clear whether it would reach the limit $\sqrt{3} \ln 2$ in very small domains.

These observations can be rationalized by considering the ratio of the two contributions to ρ'' in Eq. (33), which behaves when $R'_m \ll L' \ll 1$, as

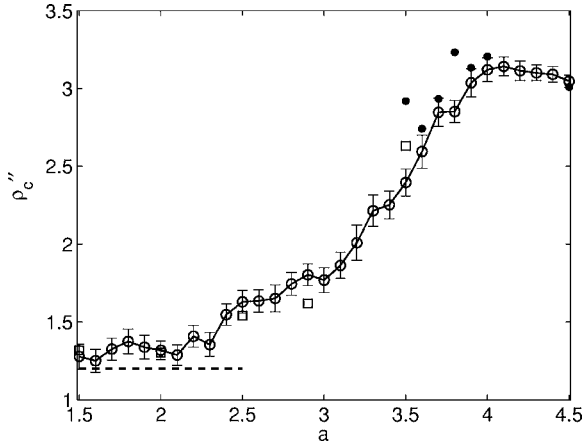

FIG. 9. The percolation thresholds ρ''_c for regular hexagons as functions of a in nonperiodic networks with $L'=0.1$, $R'_m=0.006\,25$ (○), $R'_m=0.003\,125$ (□), and $R'_m=0.0025$ (●). The vertical lines correspond to 5% variations of the percolation probability. The dashed horizontal line is the prediction of Eq. (32).

$$\frac{\eta L \langle R^2 \rangle^+}{2 \langle R^3 \rangle^-} \approx \frac{\eta |4-a|}{|3-a|} \begin{cases} \left(\dfrac{L}{2R_M} \right)^{a-3}, & 1 < a < 3, \\ 1, & 3 < a < 4, \\ \left(\dfrac{L}{2R_m} \right)^{4-a}, & 4 < a. \end{cases} \tag{34}$$

For $1 < a < 3$ the second term $\eta L \langle R^2 \rangle^+ / 2$ in ρ'' dominates, which reflects the observation that spanning by a single fracture is the most probable percolation mechanism in this range [see Figs. 7(a) and 7(b)]. Since in addition Π_1 is controlled by the largest fractures, ρ''_c is insensitive to R'_m and to the polygon shape.

In the intermediate range $3 \leqslant a \leqslant 4$, the two contributions to ρ'' are of the same order of magnitude. Percolation by a cluster of small fractures or by a single large fracture (and most probably one with a size of the order of L) are both possible; it is hard to draw hard conclusions in this transition range. Recall also that the evaluation (30) of Π_1 is inaccurate in this range of exponent, as already mentioned.

Finally, for $a > 4$, the first term dominates and ρ'' reduces to ρ'_3. With such a large exponent a, the large fractures are so uncommon that the probability of a spanning one is negligibly small, compared to the probability of the numerous fractures smaller than L to form a percolating cluster. Hence, the system reverts to the case of large domains.

This is illustrated in a different way in Fig. 9, where ρ''_c is plotted for a constant domain size $L'=0.1$ as a function of the exponent a. Three regimes can be distinguished, which correspond to the three cases in (34). For $a < 2.5$, the values of the threshold are close to the prediction (32). Between $a < 2.5$ and $a=4$, it increases rapidly and reaches a maximum at $a=4$. After $a=4$, it starts decreasing slightly. The presence of some fractures with $R \sim L$ induces finite-size effects and threshold densities larger than (24), but their probability of appearance decreases when a increases and ρ''_c progressively

decreases as well. Ultimately, ρ'' reduces to ρ'_3, and ρ''_c should converge to $\rho'_{3c}(\infty) \approx 2.4$ in Eq. (24). A transition takes place in the intermediate regime; it starts here at $a \approx 2.5$ instead of 3 as predicted by Eq. (34), because the convergence of ρ''_c to (32) is slow when a approaches 3. It is also confirmed in Fig. 9 that R'_m has no influence on ρ''_c out of the interval $3 \leqslant a \leqslant 4$.

Finally, all these observations can be summarized in the following empirical relationships whatever the fracture shapes:

$$\rho''_c \approx \begin{cases} \sqrt{3}\ln 2 \approx 1.206, & 1 \leqslant a \leqslant 2.5, \\ \sqrt{3}\ln 2 + \dfrac{a-2.5}{1.5}(3-\sqrt{3}\ln 2), & 2.5 \leqslant a \leqslant 4, \quad L' \leqslant 0.1, \\ 3, & 4 \leqslant a \leqslant 4.5. \end{cases} \tag{35}$$

For much smaller domains, the limit between the first case with a constant threshold value and the second case which is modeled by a linear increase would probably shift gradually from 2.5 to 3, and the slope in the transition region would steepen accordingly.

Any systematic numerical modeling of percolation in systems with $a > 4$ is very expensive in terms of computer time and was not done beyond what has been presented here; instead, a simple approximation of $\rho'_{3c}(L')$ by 3 is proposed which should be an acceptable estimation of the percolation threshold in this range of a and L'.

V. SCALING OF THE PERCOLATION PROPERTIES

Data obtained for large domains in Sec. III and in small domains in Sec. IV are plotted together in Fig. 10 in terms of ρ''_c as a function of L'. Recall that for $L' \geqslant 2$, ρ'' reduces exactly to ρ'_3. Note also that the exponent a remains in the range $1 < a < 3$, so that these results are fairly independent of the fracture shape.

The two regimes corresponding to the opposite limits $L' \ll 1$ and $L' \gg 1$ are clearly visible. When $L' \gg 1$, the percolation threshold decreases with L'; it converges to the limit $\rho'_{3c}(\infty)$ in Eq. (24), according to the scaling law (16). For small L', ρ''_c increases with L'; it tends towards $\sqrt{3}\ln 2 \approx 1.201$ when $L' \to 0$, as predicted by Eq. (32).

Now, consider the scaling of the percolation properties of fracture networks with a large contrast $L \gg R_m$ for the two situations $L' \gg 1$ and $L' \ll 1$.

Case $L \gg R_M$: In this regime, the percolation behavior of the fracture network is described by the scaling relations (16) and (18). In a network with $\rho'_3 < \rho'_{3c}(\infty)$, the percolation probability $\Pi(L')$ in a finite domain is always smaller than 1/2 since $\rho'_{3c}(L') > \rho'_{3c}(\infty) > \rho'_3$. Conversely, if $\rho'_3 > \rho'_{3c}(\infty)$, there exists a scale L'_c at which ρ'_3 starts exceeding $\rho'_{3c}(L')$ given by (16), and $\Pi(L')$ is larger than 1/2 for any domain with a size $L' > L'_c$.

Case $L \ll R_M$: Considering that the threshold ρ''_c for small systems remains in practice in the relatively narrow range from 1 to 3 [see Fig. 10 and Eq. (35)], the scaling behavior of the network is easily derived from Eqs. (33) and (34). The leading term of ρ'' can be expressed as

$$\rho'' \sim \rho v_{\mathrm{ex}} \begin{cases} L R_M^{3-a} R_m^{a-1}, & 1 < a < 3, \\ L^{4-a} R_m^{a-1}, & 3 < a < 4, \\ R_m^3, & 4 < a. \end{cases} \tag{36}$$

Given the density ρ, the percolation parameter ρ'' increases linearly with the system size L for $a < 3$, and as L^{4-a} for $3 < a < 4$. Therefore, provided that R_M is large enough, a critical size exists whatever ρ above which ρ'' reaches the threshold value in Eq. (35).

For $a > 4$, the percolation behavior of finite parts of the fracture network reverts to that of large domains, governed by the standard scaling relations (16)–(18), and the same considerations as for $L \gg R_M$ can be used here as well.

VI. CONCLUSIONS

Systematic numerical simulations of percolation in large domains with $L \gg R_M$ show that the normalization of the critical fracture density for polydisperse networks based on the third moment of the fracture size distribution provides a good percolation parameter. The percolation threshold ρ'_{3c} varies only slightly with R'_m which is the lower cutoff of the size distribution; little influence of the exponent a has been observed for $a < 4$, which, perhaps, can be attributed to finite size effects. The shape of polygonal fractures which do not depart too strongly from circularity is taken into account through the shape factor v_{ex}, a generalization of the result of Koudina *et al.* [27] for monodisperse networks. Furthermore, a corrective term based on a second shape factor is very successful in unifying the data for a much broader range of shapes, including very elongated polygons.

When the maximal fracture radius R_M exceeds the domain size L, the percolation probability depends on the truncated third moment $\langle R^3 \rangle^-$ for $a > 4$, and on the truncated second moment $\langle R^2 \rangle^+$ when $a < 3$. A simple combination of these two moments is proposed to form a dimensionless fracture density ρ'' which can be used to describe the percolation properties over the whole range of L and a.

Outside of a transition region with $L' \sim 1$ and $3 \leqslant a \leqslant 4$, where the competition of several mechanisms with comparable importance prevents any firm conclusion, ρ'' incorporates the influences of the fracture shape, of the domain size and of the fracture size distribution parameters R_m, R_M, and

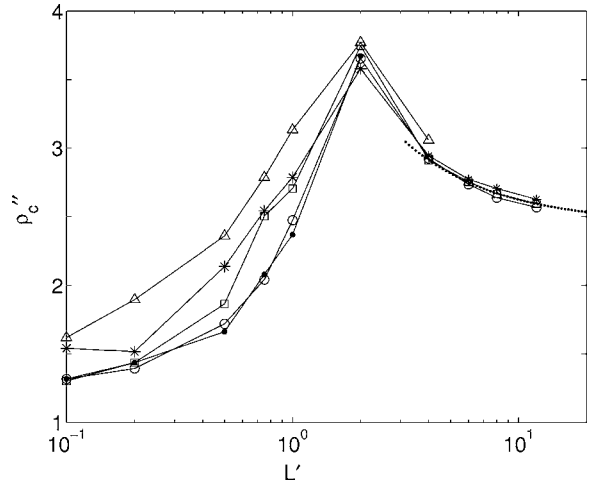

FIG. 10. The percolation thresholds for nonperiodic networks of regular hexagons as functions of L', with $R_m'=1/320$ ($L'\leqslant 2$) or $1/10$ ($L'\geqslant 4$), for $a=1.5$ (○), 2 (□), 2.5 (∗), and 2.9 (△). The dots (●) are for $a=1.5$ when $R_m'=L'/32$. The dotted line corresponds to the fit (16) of the data for $a=2$, which yields $\rho_{3c}'(\infty)=2.46$ and $\nu=0.93$.

a. It should be noted that since the parameters of the size distribution are embodied in the moments $\langle R^3\rangle^-$ and $\langle R^2\rangle^+$, the results obtained in this work for a power law can be expected to apply for other size distribution functions.

This work can be extended in many ways in order to make it still more realistic. For instance, the properties of anisotropic networks could be addressed since it is known that in most cases fracture networks can be partitioned into families of fractures whose orientations are almost constant or distributed with narrow dispersion around these orientations. However, we should mention here an observation made by Sisavath *et al.* [31]; results obtained for isotropic networks were seen to be very successful when applied to a real anisotropic network.

ACKNOWLEDGMENTS

Most computations were performed at CINES (subsidized by the MENESR). This work was also partly supported by the European contract Saltrans EVK1-Ct-2000-00062. These supports are gratefully acknowledged.

APPENDIX: ASYMPTOTICS FOR SMALL DOMAINS

Consider the intersection of the domain Ω centered at the origin of the coordinate system with an infinite plane P described by the equation

$$x\sin\theta\cos\phi + y\sin\theta\sin\phi + z\cos\theta = b,$$
$$0\leqslant\theta\leqslant\pi,\quad 0\leqslant\phi\leqslant\pi. \tag{A1}$$

The intersections of the plane P with the upper and lower planes $z=\pm L/2$ of Ω are

$$x\sin\theta\cos\phi + y\sin\theta\sin\phi = b - \frac{L}{2}\cos\theta,\quad z = L/2, \tag{A2}$$

$$x\sin\theta\cos\phi + y\sin\theta\sin\phi = b + \frac{L}{2}\cos\theta,\quad z = -L/2. \tag{A3}$$

When x varies between $-L/2$ and $L/2$, the ordinate y of the points which belong to (A2) or (A3), varies between the limits

$$\frac{1}{\sin\theta\sin\phi}\left(b - \frac{L}{2}(\cos\theta + \sin\theta|\cos\phi|)\right) \leqslant y \leqslant \frac{1}{\sin\theta\sin\phi}\left(b - \frac{L}{2}(\cos\theta - \sin\theta|\cos\phi|)\right),\quad z = L/2, \tag{A4}$$

$$\frac{1}{\sin\theta\sin\phi}\left(b + \frac{L}{2}(\cos\theta - \sin\theta|\cos\phi|)\right) \leqslant y \leqslant \frac{1}{\sin\theta\sin\phi}\left(b + \frac{L}{2}(\cos\theta + \sin\theta|\cos\phi|)\right),\quad z = -L/2. \tag{A5}$$

The intersection line (A2) passes through the upper boundary of Ω when the interval (A4) intersects the interval $-L/2\leqslant y\leqslant L/2$. This means that b should satisfy two inequalities

$$\frac{1}{\sin\theta\sin\phi}\left(b - \frac{L}{2}(\cos\theta + \sin\theta|\cos\phi|)\right) \leqslant \frac{L}{2} \tag{A6}$$

and

$$\frac{1}{\sin\theta\sin\phi}\left(b - \frac{L}{2}(\cos\theta - \sin\theta|\cos\phi|)\right) \geqslant -\frac{L}{2}. \tag{A7}$$

Similarly, the intersection line (A3) passes through the lower boundary of the domain when

$$\frac{1}{\sin\theta\sin\phi}\left(b + \frac{L}{2}(\cos\theta - \sin\theta|\cos\phi|)\right) \leqslant \frac{L}{2} \tag{A8}$$

and

$$\frac{1}{\sin\theta\sin\phi}\left(b + \frac{L}{2}(\cos\theta + \sin\theta|\cos\phi|)\right) \geqslant -\frac{L}{2}. \tag{A9}$$

The plane P intersects both upper and lower boundaries of Ω if b satisfies

$$\frac{1}{\sin\theta\sin\phi}\left(b + \frac{L}{2}(|\cos\theta| - \sin\theta|\cos\phi|)\right) \leqslant \frac{L}{2} \tag{A10}$$

and

$$\frac{1}{\sin\theta\sin\phi}\left(b - \frac{L}{2}(|\cos\theta| - \sin\theta|\cos\phi|)\right) \geqslant -\frac{L}{2} \tag{A11}$$

or equivalently

$$|b| \leqslant \frac{L\chi(\theta,\phi)}{2},\quad \chi = \sin\theta(\sin\phi + |\cos\phi|) - |\cos\theta|. \tag{A12}$$

Consider discs of radius $R \gg L$ which lie in the plane P. All discs whose centers are close to Ω intersect its opposite boundaries if the plane P does it; these centers cover an area whose surface S_p can be evaluated approximately as πR^2.

When the plane P is displaced in the normal direction, it ensures the connection between the boundaries whenever (A12) is satisfied; thus, the total possible distance of the displacement is $L\chi$. It follows that all discs whose centers belong to the volume $L\chi\pi R^2$, intersect the two opposite domain boundaries.

Let N fractures with radius R and orientation (θ, ϕ) be generated in the large volume V covering Ω ($V \gg LR^2$). The probability $p(R, \theta, \phi)$ that a fracture intersects the domain boundaries is $L\chi\pi R^2/V$. The positions of fractures in the space are independent, and the probability that neither fracture from the generated set intersects them is given by the Poisson distribution e^{-Np}. The number of fractures that have the radius R is $VF(R)\Delta R$ [cf. Eq. (7)], and N can be written as

$$N = VF(R)\Delta R \frac{\sin\theta}{2\pi}\Delta\theta\Delta\phi. \tag{A13}$$

The total probability that no fracture intersects the boundaries whatever (R, θ, ϕ) is the product of the corresponding probabilities,

$$\prod_{R,\theta,\phi} \exp\left(-L\chi\pi R^2 F(R)\Delta R \frac{\sin\theta}{2\pi}\Delta\theta\Delta\phi\right)$$
$$= \exp\left(-\sum_{R,\theta,\phi} L\chi\pi R^2 F(R)\Delta R \frac{\sin\theta}{2\pi}\Delta\theta\Delta\phi\right)$$
$$\approx \exp\left(-L\pi\lambda\int_r^{R_M} R^2 F(R)dR\right), \tag{A14}$$

where $r \ll R_M$. λ is the mean value of non-negative χ over all possible orientations (θ, ϕ),

$$\lambda = \frac{1}{2\pi}\int_0^{\pi} \sin\theta d\theta \int_0^{\pi} \chi'(\theta,\phi)d\phi = \frac{1}{\sqrt{3}} \approx 0.5774, \tag{A15}$$

$$\chi' = \begin{cases} \chi, & \chi \geq 0, \\ 0, & \chi < 0. \end{cases}$$

For polygonal fractures, the factor π in (A14) should be replaced by the dimensionless polygon area $A_p = A/R^2$, i.e., the area of an equivalent polygon inscribed in a unit disc

$$\exp\left(-LA_p\lambda\int_r^{R_M} R^2 F(R)dR\right). \tag{A16}$$

[1] M. Sahimi, *Flow and Transport in Porous Media and Fractured Rock* (VCH, New York, 1995).
[2] P. M. Adler and J.-F. Thovert, *Fractures and Fracture Networks* (Kluwer Academic, Dordrecht, 1999).
[3] National Research Council, Phys. Rev. E **57**, 4466 (2001).
[4] B. Berkowitz, Adv. Water Resour. **25**, 861 (2002).
[5] N. E. Odling, J. Struct. Geol. **19**, 1257 (1997).
[6] E. Bonnet, O. Bour, N. E. Odling, P. Davy, I. Main, P. Cowie, and B. Berkowitz, Rev. Geophys. **39**, 347 (2001).
[7] D. Stauffer and A. Aharony, *Introduction to Percolation Theory* (Taylor and Francis, Bristol, PA, 1992).
[8] P. C. Robinson, J. Phys. A **16**, 605 (1983).
[9] P. C. Robinson, J. Phys. A **17**, 2823 (1984).
[10] E. Charlaix, E. Guyon, and N. River, Solid State Commun. **50**, 999 (1984).
[11] O. Huseby, J.-F. Thovert, and P. M. Adler, J. Phys. A **30**, 1415 (1997).
[12] J.-R. de Dreuzy, P. Davy, and O. Bour, Phys. Rev. E **62**, 5948 (2000).
[13] W. R. Rossen, Y. Gu, and L. W. Lake, Connectivity and permeability in fracture networks obeying power-law statistics, paper SPE 59720 presented at the 2000 SPE Permian Basin Oil and Gas Recovery Conference held in Midland, Texas, 21–23 March 2000 (unpublished).
[14] B. Lorenz, I. Orgzall, and H.-O. Heuer, J. Phys. A **26**, 4711 (1993).
[15] B. Berkowitz, Math. Geol. **27**, 467 (1995).
[16] D. Dhar, Physica A **242**, 341 (1997).
[17] K. R. Mecke and A. Seyfried, Europhys. Lett. **58**, 28–34 (2002).
[18] R. Consiglio, D. R. Baker, G. Paul, and H. E. Stanley, Physica A **319**, 49 (2003).
[19] V. V. Mourzenko, J.-F. Thovert, and P. M. Adler, Phys. Rev. E **69**, 066307 (2004).
[20] A. R. Piggott, J. Geophys. Res., & Solid Earth **102**, 18 121 (1997).
[21] B. Berkowitz and P. M. Adler, J. Geophys. Res., & Solid Earth **103**, 15339 (1998).
[22] I. Balberg C. H. Anderson, S. Alexander, and N. Wagner, Phys. Rev. B **30**, 3933 (1984).
[23] A. Isihara, J. Chem. Phys. **18**, 1446 (1950).
[24] P. G. De Gennes, *The Physics of Liquid Crystals* (Oxford University Press, New York, 1976).
[25] L. A. Santalo, *Integral Geometry and Geometric Probability* (Addison Wesley, Reading, 1976).
[26] R. Schneider and W. Weil, *Integralgeometrie* (Teubner, Stuttgart, 1992).
[27] N. Koudine, R. Gonzalez Garcia, J.-F. Thovert, and P. M. Adler, Phys. Rev. E **57**, 4466 (1998).
[28] E. J. Garboczi, K. A. Snyder, J. F. Douglas, and M. F. Thorpe, Phys. Rev. E **52**, 819 (1995).
[29] R. Florian and Z. Neda, cond-mat/0110067 (unpublished).
[30] M. O. Saar and M. Manga, Phys. Rev. E **65**, 056131(6) (2002).
[31] S. Sisavath, V. Mourzenko, P. Genthon, J.-F. Thovert, and P. M. Adler, Geophys. J. Int. **157**, 917–934 (2004).
[32] J.-F. Thovert and P. M. Adler, Geophys. Res. Lett. **31**, L22502 (2004).